Size effect on magnetic coupling in all-ferromagnetic superlattices

P. Padhan and W. Prellier

Articles you may be interested in

Raman spectra and magnetization of all-ferromagnetic superlattices grown on (110) oriented SrTiO3
Appl. Phys. Lett. **104**, 092406 (2014); 10.1063/1.4867509

Effect of superconducting spacer layer thickness on magneto-transport and magnetic properties of La0.7Sr0.3MnO3/YBa2Cu3O7/La0.7Sr0.3MnO3 heterostructures
J. Appl. Phys. **115**, 013901 (2014); 10.1063/1.4861139

Magnetic proximity effect in Pr0.5Ca0.5MnO3/La0.7Sr0.3MnO3 bilayered films
Low Temp. Phys. **38**, 41 (2012); 10.1063/1.3677235

Antiferromagnetic coupling and enhanced magnetization in all-ferromagnetic superlattices
Appl. Phys. Lett. **88**, 192509 (2006); 10.1063/1.2202690

Effect of ferromagnetic/antiferromagnetic interfaces on the magnetic properties of La 2/3 Sr 1/3 Mn O 3/Pr 2/3 Ca 1/3 Mn O 3 superlattices
J. Appl. Phys. **99**, 08C903 (2006); 10.1063/1.2170058
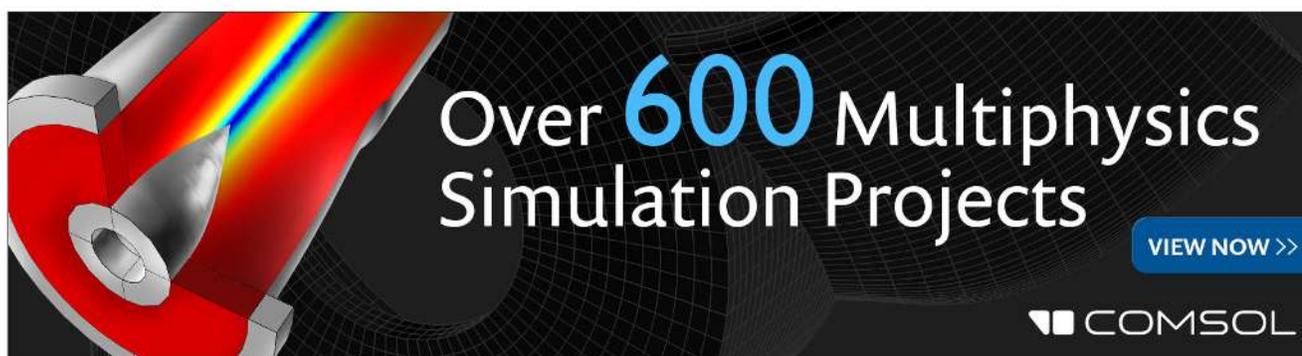
Size effect on magnetic coupling in all-ferromagnetic superlattices

P. Padhan[1,a)] and W. Prellier[2]

[1]*Department of Physics, Indian Institute of Technology Madras, Chennai 600036, India*
[2]*Laboratoire CRISMAT, CNRS UMR 6508, ENSICAEN, 6 Bd du Maréchal Juin, F-14050 Caen Cedex, France*

The switching of ferromagnetic-to-antiferromagnetic coupling of magnetization in the superlattices consisting of two ferromagnetic metals $La_{0.7}Sr_{0.3}MnO_3$ (LSMO) and $SrRuO_3$ (SRO) grown on (001) oriented $SrTiO_3$ has been observed by changing the orientation of the field from out–of–plane to in–plane direction. Such switching of magnetic coupling strongly depends on the stacking order of $La_{0.7}Sr_{0.3}MnO_3$ and $SrRuO_3$ layers in the superlattice of 20 unit cell (u.c.)/ n (= 3 or 5) u.c. thickness configuration. This is explained by the structural distortion in the MnO_6 and RuO_6 octahedra along the out-of-plane direction due to the observed stress. © *2011 American Institute of Physics*. [doi:10.1063/1.3673295]

Several interesting magnetic properties of the interfaces of $La_{0.7}Sr_{0.3}MnO_3$ (LSMO) and $SrRuO_3$ (SRO) multilayers have been reported.[1–5] For instance, Ke *et al.*[1] have observed exchange bias effect in the magnetic structure consisting of FM bilayer composed of $La_{0.67}Sr_{0.33}MnO_3$ and $SrRuO_3$. Very recently, Ziese *et al.*[2] have studied $La_{0.7}Sr_{0.3}MnO_3$ and $SrRuO_3$ superlattices and observed strong antiferromagnetic interlayer coupling depended delicately on magnetocrystalline anisotropy. These superlattices also show inverted hysteresis loop due to strong exchange bias between $La_{0.7}Sr_{0.3}MnO_3$ and $SrRuO_3$.[3] While Thota *et al.* have observed crossover between inverse and conventional magnetic entropy changes with temperature.[5] In our earlier study, we found enhanced magnetization and antiferromagnetic coupling in $La_{0.7}Sr_{0.3}MnO_3$ and $SrRuO_3$ superlattices.[4] These observations are attributed to the possible modification in the stereochemistry of the Ru and Mn ions in the interfacial region. We have further studied the magnetic properties of the LSMO-SRO superlattices grown on (001) oriented $SrTiO_3$ (STO) for both stacking sequences of constituents with 20 u.c./n u.c. thickness configuration. The enhanced magnetization and antiferromagnetic coupling strongly indicates the influence of stacking sequences. In addition, these samples also show the switching of ferromagnetic coupling to antiferromagnetic coupling by changing the orientation of magnetic field from in–plane to out–of–plane direction. Therefore, this study may open a constructive approach for buffer layer and electrode used in spintronic devices and for the magnetic refrigeration application.[5]

The multitarget pulsed laser deposition technique has been used to grow thin films of LSMO and SRO and their superlattice structures on (001) oriented STO substrates. The detail of the deposition process has been described previously.[4] The deposition rates for SRO and LSMO layer are calibrated individually for each laser pulse of energy density $\sim$3 J/cm^2 and it seems to be almost the same $\sim$0.73 Å/pulse. Series of superlattice structures with STO/20-u.c. LSMO/ n-u.c. SRO and STO/20-u.c. SRO/n-u.c. LSMO configurations for n = 3 and 5 were synthesized by repeating the

bilayer, 15 times. Note that in all samples, the bottom layer is 20 u.c. thick while the top layer is either 3 u.c. or 5 u.c. thick. The periodic modulations in composition were calculated using established deposition rates of LSMO and SRO obtained from the positions of superlattice reflections in x-ray θ-2θ scans. The epitaxial growth and structural characterization of the multilayer and single layer films were performed using x-ray diffraction. The magnetization (M) measurements were carried out using a superconducting quantum interference device based magnetometer (Quantum Design MPMS-5). The field-cooled magnetization is measured by cooling the sample below room temperature in the presence of magnetic fields along the [100] and [001] directions of the STO substrate. The orientation of the magnetic field during the field-cooled measurements remains similar to that of the cooling field.

The pseudocubic lattice parameter of STO (3.905 Å) is smaller than that of the SRO (3.93 Å) but larger than that of the LSMO (3.88 Å). Thus, STO provides in-plane tensile stress and compressive stress for the epitaxial growth of LSMO and SRO with lattice mismatch -0.64% and $+0.64\%$, respectively. However, the LSMO-SRO superlattice stabilizes pseudocubic phases of these perovskites on STO substrate irrespective of the bottom layer. The θ-2θ x-ray scan of the superlattices with n = 3, around the (001) reflection of STO, are shown in the Fig. 1. We have carried out quantitative refinement of x-ray diffraction profile of these superlattice structures using DIFFAX program.[4] The simulated profiles of the superlattice with n = 3 around the (001) reflection of STO are also plotted in the Fig. 1. The simulated profile using the calibrated thickness is in good agreement with the position of the Kiessig fringes and their relative intensity ratio. Though we have observed up to 5th order satellite peaks, only 0th and 1st order satellite peaks are shown to have a clear view of the influence of observed strain of the superlattice structure. The out-of-plane lattice parameters "c" calculated from 0th order peak positions of STO/[20-u.c. LSMO/n-u.c. SRO]$_{x15}$ and STO/[20-u.c. SRO/n-u.c. LSMO]$_{x15}$ superlattices with n = 3 and 5 are shown in the Table I. The observed out-of-plane lattice parameter of STO/[20-u.c. LSMO/n-u.c. SRO]$_{x15}$ superlattice with n = 3 is smaller than that of the bulk LSMO, so the in-plane lattice parameter of the same superlattice is larger

a)Author to whom correspondence should be addressed. Electronic mail: padhan@iitm.ac.in.
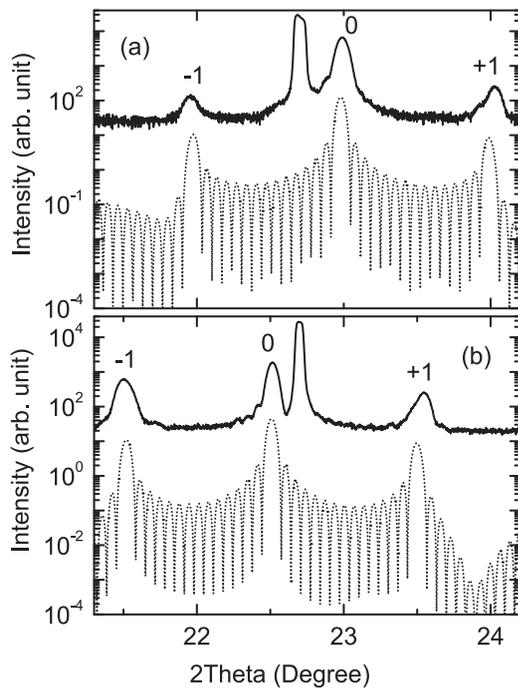
FIG. 1. The experimental (solid line) and simulated (DIFFaX) (dotted line) θ-2θ x-ray diffraction profiles of (a) (001)STO/[20-u.c. LSMO/3-u.c. SRO]$_{x15}$ and (b) (001)STO/[20-u.c. SRO/3-u.c. LSMO]$_{x15}$ superlattices. The (001) Bragg's reflection of STO as well as the satellite peaks (0th and $\pm$ 1st orders) are indicated.

than that of the LSMO assuming the conservation of volume. Thus, this superlattice has in-plane tensile stress as expected from the lattice mismatch between the STO and LSMO. Similarly, the presence of in-plane compressive stress in STO/[20-u.c. SRO/n-u.c. LSMO]$_{x15}$ superlattices with $n = 3$ is confirmed from the observed "c" of this superlattice. Furthermore, the decrease in the change in out-of-plane lattice parameter "Δc" i.e., the decrease of observed stress irrespective of the bottom layer, strongly support the structural change in the superlattice due to the size effect. This indicates the relaxation of the in-plane stress due to the increase in the bilayer thickness in LSMO-SRO superlattice systems with both the stacking orders.

Figure 2 shows the field cooled (FC) temperature dependent magnetization M(T) curves of four superlattices. These measurements were carried out in-presence of 0.1 T field oriented along the [001] and [100] directions of STO. The M(T) curves show the onset of spontaneous magnetization of the STO/[20-u.c. LSMO/n-u.c. SRO]$_{x15}$ superlattices (Figs. 2(a) and 2(b)) occurs at $\sim$360 K while it is observed at relatively lower temperature $\sim$320 K for STO/[20-u.c. SRO/n-u.c.

LSMO]$_{x15}$ superlattices. The difference in the T$_C$ of the superlattices with both stacking order sequences of the LSMO and SRO layers is attributed to the finite size effect (i.e., the reduced dimensionality along the out-of-plane direction which causes the cutoff of some characteristic length). As the superlattices are cooled further below $\sim$320 K, their M(T) curves are significantly diverse for different spacer layer, spacer layer thickness, and the orientation of the magnetic field. For example, the in-plane magnetization of STO/[20-u.c. LSMO/3-u.c. SRO]$_{x15}$ superlattice increases gradually on cooling below $\sim$320 K up to $\sim$40 K but then decreases down to lowest temperature, while the out-of-plane M(T) shows a distinct cusp around 60 K (T$_N$ Neel temperature). The drop in magnetization, at a temperature which we have marked T$_N$, could be due to disordered interface.[4] A similar AFM exchange coupling has been observed in La$_{0.6}$Sr$_{0.4}$MnO$_3$/Sr$_{0.7}$Ca$_{0.3}$RuO$_3$/La$_{0.6}$Sr$_{0.4}$MnO$_3$ trilayers by Uozu et al.[6] and in La$_{0.67}$Sr$_{0.33}$MnO$_3$/SrRuO$_3$ bilayers by Ke et al.[1] However, as the SRO layer thickness increases to 5 u.c., the T$_N$ of in-plane as well as out-of-plane M(T) is shifted to higher temperature ($\sim$110 K). In addition, a plateau is observed around $\sim$200 K in the out-of-plane M(T) curve. The values of T$_N$ and T$_C^*$ (T$_C^*$ is the temperature at which the SRO layer becomes ferromagnetic since the magnetization rises sharply below this temperature) of the STO/[20-u.c. LSMO/5-u.c. SRO]$_{x15}$ superlattice is relatively lower and higher respectively compared to the values observed in the Ref. 4. In order to verify the origin of this change in T$_N$ and T$_C^*$, we have covered the STO/[20-u.c. LSMO/5-u.c. SRO]$_{x15}$ superlattice with 20 u.c. thick LSMO and found similar magnetic properties as observed in Ref. 4. This experiment concluded that the 20 u.c. thick LSMO top layer provides uniform interfaces to the spacer layers has strong influence on the magnetic properties of the STO/[20-u.c. LSMO/n-u.c. SRO]$_{x15}$ superlattice. The observed T$_N$ in M(T) for both the orientations of magnetic field indicates the presence of antiferromagnetic coupling between the LSMO and SRO. In contrast, the T$_N$ ($\sim$ 150 K) and T$_C^*$ ($\sim$ 150 K) are observed in the in-plane and out-of-plane M(T), respectively, as the order of LSMO and SRO is reversed in the superlattice with same thickness configuration. Note that no significant change of T$_N$ and T$_C^*$ for different values of LSMO spacer layer thickness in the STO/[20-u.c. SRO/n-u.c. LSMO]$_{x15}$ superlattices with $n = 3$ and 5 is observed, although there is a remarkable variation of magnetic behavior below the T$_N$ and T$_C^*$ in the in-plane and out-of-plane M(T), respectively. The observed M(T) curve indicates that the coupling between SRO and LSMO is antiferromagnetic in-the-plane and ferromagnetic along out-of-plane of the superlattices.

The magnetic properties of these superlattices at 10 K are also investigated for field oriented along the [001] and [100]

TABLE I. Out-of-plane lattice parameter "c" of various superlattices and the percentage of change of the "c" with respect to the lattice parameter "c$_b$" of the bottom layer in bulk form. The error of "c" and "$\Delta c/c_b$" calculated from experimental uncertainty (i.e., least count 0.001° of x-ray diffractometer) and the error due to the uncertainty of the fit to the 0th order peak position of the superlattice.

| Sample	Out-of-plane lattice parameter (Å)		($\Delta c/c_b$) (%)	
	n = 3	n = 5	n = 3	n = 5
STO/(20 u.c.)SRO/(n u.c.)LSMO	3.9458 $\pm$ 0.00018	3.9376 $\pm$ 0.00022	0.402 $\pm$ 0.0045	0.193 $\pm$ 0.0056
STO/(20 u.c.)LSMO/(n u.c.)SRO	3.8653 $\pm$ 0.00018	3.8731 $\pm$ 0.00018	0.378 $\pm$ 0.0045	0.177 $\pm$ 0.0045
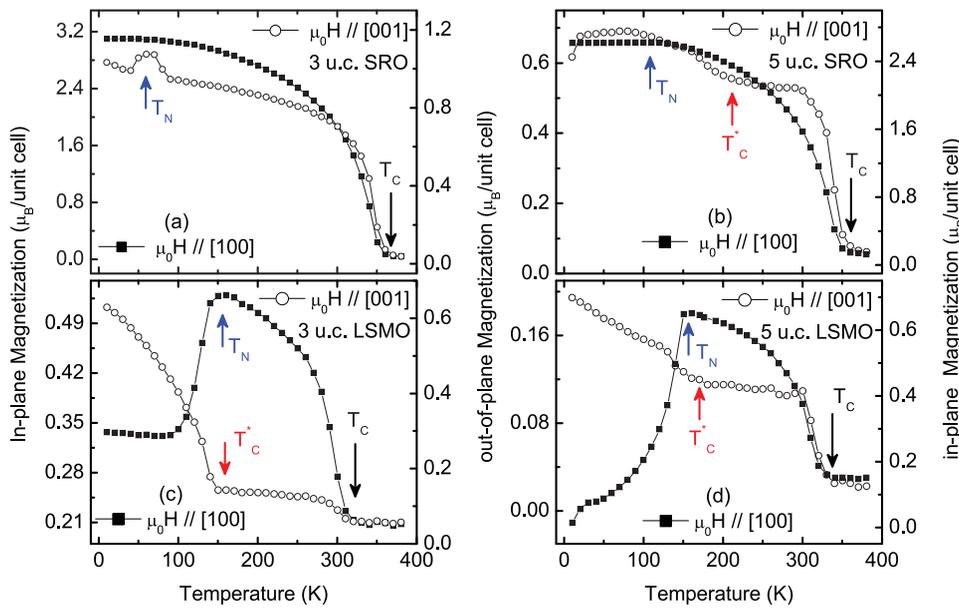
FIG. 2. (Color online) Temperature dependent 0.1 tesla field cooled magnetization of (a) (001)STO/[20-u.c. LSMO/3-u.c. SRO]$_{x15}$, (b) (001)STO/[20-u.c. LSMO/5-u.c. SRO]$_{x15}$, (c) (001)STO/[20-u.c. SRO/3-u.c. LSMO]$_{x15}$, and (d) (001)STO/[20-u.c. SRO/5-u.c. LSMO]$_{x15}$ superlattices with field oriented along the plane and out-of-plane. The arrows indicate the T_C, T_C*, and T_N.

directions of STO. The zero-field-cooled magnetization of these superlattices at various field M(H) is shown in the Fig. 3. The diamagnetic contribution of the substrate to M(H) of these superlattices has been subtracted. The M(H) of STO/[20-u.c. LSMO/n-u.c. SRO]$_{x15}$ superlattices (Figs. 3(a) and 3(b)) exhibit magnetic anisotropy similar to that of the LSMO.[7] The saturation magnetization (M_S) extracted from the M(H) of the superlattice with 3 and 5 u.c. SRO spacer is ~3.5 and ~3.0 μ_B/u.c., respectively. The observed lower values of M_S compared to the reported values[4] is attributed to the influence of 20 u.c. thick LSMO top layer. Nevertheless, the superlattice with 3 u.c. SRO spacer shows higher M_S compared to the M_S (~3.11 μ_B/u.c.) calculated from the spin only M_S of the LSMO (3.34 μ_B/Mn (Ref. 8)) and SRO (1.6 μ_B/Ru (Ref. 9)) while the superlattice with 5 u.c. thick SRO spacer layer shows M_S close to that of the calculated M_S (~2.99 μ_B/u.c.). The enhanced magnetization and the higher value of

T_C* could be due to the modification of the charge states of the Ru and Mn ions[10] at the interfaces, and thereby an increase in the effective thickness of the interfacial layer in the superlattice.[4] On the other hand, as the stacking order of LSMO and SRO layer in the superlattice is reversed with same thickness configuration, the M(H) of both the superlattices show clear ferromagnetic hysteresis (Figs. 3(c) and 3(d)). Indeed, in-plane M(H) of both superlattices show double hysteresis loop. At 5 tesla, the magnetization reaches ~1.5 and ~1.2 μ_B/u.c. for the superlattice with 3 and 5 u.c. thick LSMO spacer layer, respectively, but does not fully saturate even at 5 tesla field [unlike in the case of LSMO-SRO superlattice (Ref. 2)]. The observed monotonic increase of magnetization with the magnetic field even at 5 tesla of the STO/[20-u.c. SRO/n-u.c. LSMO]$_{x15}$ superlattices suggests the presence of spin canting, spin reorientation, and spin pinning/bias.[11]
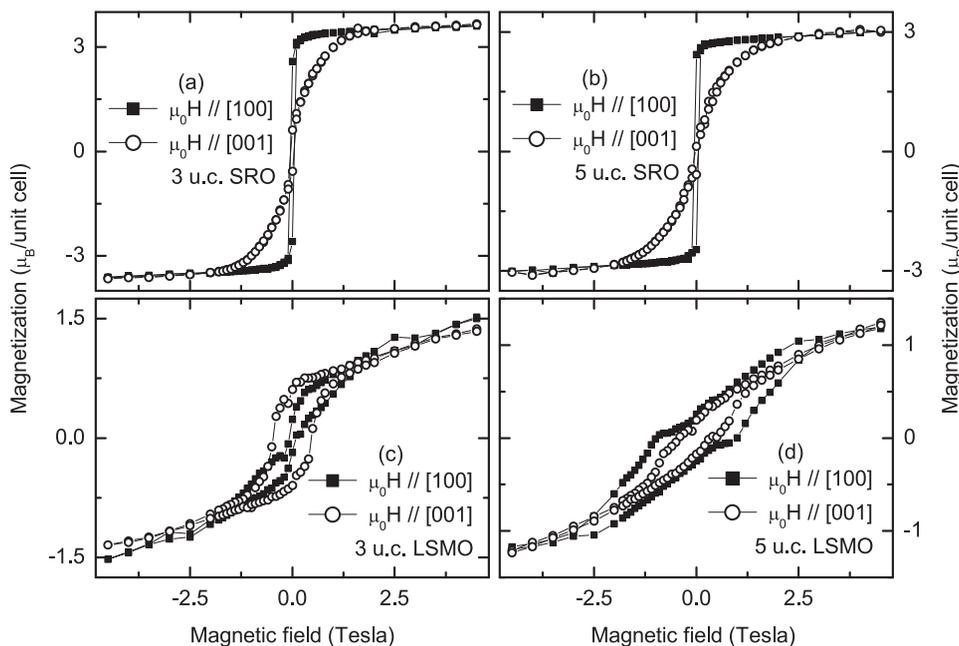

FIG. 3. Field dependent magnetization at 10 K with field oriented along the plane and out-of-plane of (a) (001)STO/[20-u.c. LSMO/3-u.c. SRO]$_{x15}$, (b) (001)STO/[20-u.c. LSMO/5-u.c. SRO]$_{x15}$, (c) (001)STO/[20-u.c. SRO/3-u.c. LSMO]$_{x15}$, and (d) (001)STO/[20-u.c. SRO/5-u.c. LSMO]$_{x15}$ superlattices.

The observed stress, M(T) and M(H) of the LSMO–SRO superlattices strongly depends on the stacking order of LSMO and SRO layer for the 20 u.c./n u.c. thickness combination. Though the observed variation in the stress is obvious due to the size effect, its influence on the magnetic properties could be vital due to the distortion in the MnO_6 (Ref. 12) and RuO_6 (Ref. 13). The switching of ferromagnetic to antiferromagnetic orientation of magnetization of the STO/[20-u.c. SRO/n-u.c. LSMO]$_{x15}$ superlattices by changing the field from out–of–plane to in–plane direction is attributed to the competing effect of distortion in the MnO_6 and RuO_6 octahedra due to observed stress.

In conclusion, using two metal-like ferromagnets $La_{0.7}Sr_{0.3}MnO_3$ and $SrRuO_3$ in the superlattices, we demonstrate that the switching of ferromagnetic to antiferromagnetic orientation of magnetization can be induced by changing the field from out–of–plane to in–plane direction. Such switching strongly depends on the stacking order of LSMO and SRO layer in the superlattice of 20 u.c./n u.c. thickness configuration. This is explained by the possibility of the competing effect of distortion in the MnO_6 and RuO_6 due to the observed stress.

[1]X. Ke, M. S. Rzchowskia, J. Belenky, and C. B. Eom, Appl. Phys. Lett. **84**, 5458 (2004).

[2]M. Ziese, I. Vrejoiu, E. Pippel, P. Esquinazi, D. Hesse, C. Etz, J. Henk, A. Ernst, I. V. Maznichenko, W. Hergert *et al.*, Phys. Rev. Lett. **104**, 167203 (2010).

[3]M. Ziese, I. Vrejoiu, and D. Hesse, Appl. Phys. Lett. **97**, 052504 (2010).

[4]P. Padhan, W. Prellier, and R. C. Budhani, Appl. Phys. Lett. **88**, 192509 (2006).

[5]S. Thota, Q. Zhang, F. Guillou, U. Lüders, N. Barrier, W. Prellier, A. Wahl, and P. Padhan, Appl. Phys. Lett. **97**, 112506 (2010).

[6]Y. Uozu, T. Nakajima, M. Nakamura, Y. Ogimoto, M. Izumi, and K. Miyano, Appl. Phys. Lett. **85**, 2875 (2004).

[7]J.-H. Park, E. Vescovo, H.-J. Kim, C. Kwon, R. Ramesh, and T. Venkatesan, Nature **392**, 794 (1998).

[8]G. Banach, R. Tyer, and W. M. Temmerman, J. Magn. Magn. Mater. **272**, 1963 (2004).

[9]D. Singh, J. Appl. Phys. **79**, 4818 (1996).

[10]C. Martin, A. Maignan, M. Hervieu, C. Autret, B. Raveau, and D. I. Khomskii, Phys. Rev. B **63**, 174402 (2001).

[11]M. Izumi, Y. Ogimoto, Y. Okimoto, T. Manako, P. Ahmet, K. Nakajima, T. Chikyow, M. Kawasaki, and Y. Tokura, Phys. Rev. B **64**, 064429 (2001).

[12]C. Aruta, G. Ghiringhelli, A. Tebano, N. G. Boggio, N. B. Brookes, P. G. Medaglia, and G. Balestrino, Phys. Rev. B **73**, 235121 (2006).

[13]Y. Shirako, H. Satsukawa, H. Kojitani, T. Katsumata, M. Yoshida, Y. Inaguma, K. Hiraki, T. Takahashi, K. Yamaura, E. Takayama-Muromachi *et al.*, J. Phys.: Conf. Ser. **215**, 012038 (2010).